



Heat transfer enhancement of two-phase droplet flow in microtube: a phase-field simulation study

V. C. Teixeira¹ · F. S. Forte Neto¹ · G. M. Guerra² · A. G. B. da Cruz¹

Received: 15 April 2021 / Accepted: 3 February 2022 / Published online: 4 March 2022

© The Author(s), under exclusive licence to The Brazilian Society of Mechanical Sciences and Engineering 2022

Abstract

Using the Navier–Stokes–Cahn–Hilliard model coupled with the energy equation, we investigate the heat transfer enhancement of two-phase immiscible droplet flow through a co-flow droplet formation device in a dripping regime. Numerical results show a significant heat transfer enhancement at the position of the droplet. The effect of droplet size and flow rate on the heat transfer of two-phase flow is analyzed and suggests an optimal flow rate ratio that produces the best thermal transport. A flow-type parameter, which describes the relative strength of stretching and rotation rates, is extracted to represent the recirculation strength in the two-phase droplet flows. At last, we indicate a capillary number in which the heat transfer enhancement achieved the best results when considering the pressure loss over the microtube.

Keywords Droplets · Phase-field model · Heat transfer enhancement · Co-flowing microtube

List of symbols

Nu	Nusselt number
Ca	Capillary number
Pe	Peclet number
Re	Reynolds number
\mathbf{v}	Velocity vector (m/s)
p	Pressure (Pa)
T	Temperature (K)
T_b	Bulk mean temperature (K)
$T_{w,z}$	Wall temperature (K)
R	Microchannel radius (μm)
m	Mobility ($\text{m}^3\cdot\text{s}/\text{kg}$)
Q	Volumetric flow rate ($\mu\text{l}/\text{s}$)

c_v	Specific heat capacity at constant volume ($\text{J}/\text{kg K}$)
k	Thermal conductivity ($\text{W}/\text{m K}$)
\bar{v}	Average velocity (m/s)

Greek symbols

φ	Phase-field variable
μ	Chemical potential (J/m^3)
ν	Viscosity ($\text{Pa}\cdot\text{s}$)
ρ	Density (kg/m^3)
α	Flow rate ratio
σ	Surface tension (N/m)
κ	Temperature coefficient ($\text{N}/\text{m K}$)
λ	Mixing energy per unit length (J/m)
ε	Interfacial thickness (m)
χ	Mobility tuning parameter ($\text{m}\cdot\text{s}/\text{kg}$)
ϑ	Dimensionless temperature

Subscript

c	Continuous phase
d	Dispersed phase

Technical Editor: Francis HR Franca.

✉ V. C. Teixeira
victor.c.teixeira@gmail.com

F. S. Forte Neto
fforteneto@gmail.com

G. M. Guerra
gguerra@id.uff.br

A. G. B. da Cruz
aguicruz@ufpa.br

¹ Postgraduate Program of Mechanical Engineering/ITEC, Universidade Federal do Pará, Belém, Brazil

² Department of Mechanical Engineering - TEM/PGMEC, Universidade Federal Fluminense, Niterói, Brazil

1 Introduction

Two-phase flows of immiscible liquids appear in the context of several applications. Flows involving deformable droplets and slugs in a liquid carrier phase have the potential of enhancing heat transfer in microfluidic devices, as presented by Fischer et al. [1] and Bordbar et al. [2] in their study of thermal convective enhancement of microchannel heat

sinks for electronics cooling. They observed that the droplets transport in a continuous phase, an enhanced convective thermal transport occurs as a result of blockage effects between subsequent droplets, causing vorticity rates and velocity distribution in the liquid slugs (see, e.g., Muzychka et al. [3]). Works related to the dynamics of temperature-actuated droplets have focused mainly on the generation and transport of liquid droplets (see, e.g., [4–6]). Most of these works have restricted their investigations through T-junctions and flow-focusing droplet formation devices that account for the effects of temperature-dependent viscosity and interfacial tension on the velocity and volume change (see [6, 7]), and rapid mixing within individual droplets [8]. Khater et al. [9] emphasized in their study that the physical behavior of dispersed droplets in response to a temperature change or heating source placed downstream far from the droplets ejection section requires further research on characterizing droplets thermal behavior within microchannels.

The main characteristic of two-phase droplet flows is the presence of a deformable interface separating the immiscible phases. Two-phase structures in immiscible fluids flows are subject to a high degree of topological change of the fluid interfaces (e.g., coalescence or breakup of droplets). Such topological changes make the interface tracking a challenging task (see [10, 11]). Difficulties in simulating the topological evolution of deformable interfaces come from the fact that its movement follows a material description, while the transport process is predicted from spatial descriptions; to merge these two frameworks are not straightforward (Santra et al. [11]). Standard strategies for tracking interfaces are the front-tracking method (see, e.g., [12–15]), sharp interface methods such as volume-of-fluid [2, 16, 17] and level-set [18–20]), and diffuse interface method (see [21, 22]); each one presenting advantages and drawbacks in representing the interface. As emphasized by Santra et al. [11], for example, the level-set and volume-of-fluid methods cannot handle the rapid spatial change in the micro-scale topology of the liquid interface. Standard treatments of two-phase droplet flows consider the interface between two phases as discontinuity surfaces. In contrast, the diffuse interface method assumes a three-dimensional transition zone separating the two phases; the material properties characterizing the bulk phases and interfacial forces vary smoothly. The diffuse interface method uses free energy for describing the interface that depends on the intermolecular forces of the components (Santra et al. [11]). The diffuse interface method provides a consistent thermodynamic formulation, which allows capturing topological changes; see Gurtin et al. [21]. Further, the diffuse interface method allows for the modeling of interfacial phenomena without *a priori* assumptions on the shape of the moving interface, which is represented by a thin, smooth transition layer; this is achieved by introducing a phase-field variable, which requires an evolution equation.

In this view, the Cahn–Hilliard equation [23, 24] or its non-conservative counterpart the Allen–Cahn equation [25] are commonly used to describe the dynamic evolution of the phase-field variable. When coupled to the Navier–Stokes equations, introduce interfacial stress given by the chemical potential and the gradient of the phase-field parameter (see Gurtin et al. [21]).

Phase-field modeling based on the Navier–Stokes–Cahn–Hilliard has been used for capturing the interfacial phenomena of multicomponent and multiphase flow within microfluidics, including droplet dynamics in unbounded flow, such as droplet formation and breakup; see, e.g., [26–31] or the presence of solid boundaries. De Menech [26] studied modeling of droplet breakup in a microfluidic T-shaped junction with a phase-field model in the hydrodynamic regime where capillary and viscous stresses dominate over inertial forces within microfluidic devices. In a recent study by Bai et al. [32], a three-dimensional droplet generation in a flow-focusing microchannel is studied by performing a phase-field method based on the Navier–Stokes equations coupled with the Cahn–Hilliard equation. These works have studied the dynamics of generation and transport of droplets in T-junction, co-flowing, and contraction-expansion microfluidic devices. Analysis of droplets transport within microfluidics is complicated due to the need for three-dimensional simulating of droplets. According to Khater et al. [9], most of the droplet generation and transport are limited to two-dimensional simulations aiming to study heat transfer enhancement and characterize internal vortices in liquid plugs in microchannels and within the droplets through the Marangoni effect (see, e.g., [1, 33]).

In this work, we study the thermal behavior of two-phase droplet transport within a co-flowing microtube subjected to a temperature change. Further, we analyze the effect of two-phase droplet frequency in terms of the flow rate ratio and recirculation between droplets on the heat transfer enhancement. For that, we use an axisymmetric phase-field model based on the Navier–Stokes–Cahn–Hilliard equations coupled with the heat equations for simulating droplets transport in the co-flowing microchannel.

The model is solved using a mixed finite element method implemented in the software COMSOL Multiphysics. Then, the model is applied to investigate the effects of the droplets dynamics on the temperature distribution within the microchannel. Further, we study the thermal convective enhancement within microchannel by the vortices in the continuous phase due to liquid–liquid interfaces. We assume a simplified model by considering droplets formation in a co-flowing microchannel and heat transfer as a Graetz problem.

We have structured the remainder of this work as follows. In Sect. 2, we introduce the problem definition and mathematical modeling for the two-phase flow. Then, in Sect. 3, we describe the numerical details to solve the physical

problem using a mixed finite element implementation in the COMSOL Multiphysics. We present results and discussions in Sect. 4 and the conclusion in Sect. 5.

2 Problem definition and phase-field equations

2.1 Geometry of co-flowing microtube

We adopted a co-flowing microtube geometry to reproduce a droplet two-phase flow regime studied by Fischer et al. [1]. The co-flowing liquid stream controls the generation and transport of dispersed droplets in a dripping regime (see, e.g., [34]), such that hydrodynamic forces are employed to control the pinching of the liquid–liquid interface, modifying the size of the droplets, and generation frequency. The geometry of the cylindrical microchannel, which comprises two aligned capillary tubes, is shown in Fig. 1), with the radius of the carrier cylindrical microchannel and injection capillary tube are $R = 500 \mu\text{m}$ and $r_i = 0.2R$, respectively. The total length is $50R$ to ensure full thermal development of droplet two-phase flow, which can also ensure the fully developed flow in the case of single-phase flow. The wall temperature distribution of the microtube is set to be 300 K for $-30R < z < 0$ and 340 K for $0 < z < 20R$, respectively.

Driven by pressure loads, the dispersed droplets (phase 2) flow into the continuous liquid (phase 1). A train of droplets is formed, detached, and immersed into the isothermic region of the capillary tube, $-30R < z < 0$. As they move with the continuous liquid, the flow develops around the droplets deforming the interface between the two phases and their surrounding, immiscible liquid. After that, the train of droplets enters into the thermally developing region of the microtube. Heat transfer of a single-phase-laminar flow in the cylindrical microchannel follows the classical Graetz problem; see, e.g., [35].

2.2 Phase-field equations

We apply a particular version of the Navier–Stokes–Cahn–Hilliard equations introduced in Gurtin et al. [21], which were originally developed for predicting separation of two-phase binary fluids, to study the following physical process occurring in the co-flowing cylindrical microchannel (Fig. 1): Droplet

dynamics (formation, breakup, coalescence, and transport), convective heat transfer, and two-phase flow of immiscible liquids. In short, we use the phase-field model based on the Cahn–Hilliard equation to capture the interface between droplet and continuous phase. The Navier–Stokes and continuity equations are solved to simulate the flow field. Thus, the governing equations are given by

$$\left. \begin{aligned} \rho \dot{\mathbf{v}} &= -\text{grad } p + \text{div}(\nu(\text{grad } \mathbf{v} + (\text{grad } \mathbf{v})^T)) + \mu \text{grad } \varphi, \\ \text{div } \mathbf{v} &= 0, \\ d \frac{\partial \varphi}{\partial t} + \mathbf{v} \cdot \text{grad } \varphi &= m \Delta \mu, \\ \mu &= f'(\varphi) - \lambda \Delta \varphi, \end{aligned} \right\} \quad (1)$$

which must be solved for the gross velocity field \mathbf{v} , pressure p , phase-field variable φ , and chemical potential μ ; where $\dot{\mathbf{v}} = \left(\frac{\partial \mathbf{v}}{\partial t} + \mathbf{v} \cdot \text{grad } \mathbf{v} \right)$ denotes the material-time derivative, Δ denotes the Laplacian operator, and m is the mobility. The term $\mu \text{grad } \varphi$ accounts for surface tension force on the interface between two phases.

In addition, we coupled the phase-field model to the energy equation,

$$\rho c_v \left(\frac{\partial T}{\partial t} + \mathbf{v} \cdot \text{grad } T \right) = \text{div}(k \text{grad } T), \quad (2)$$

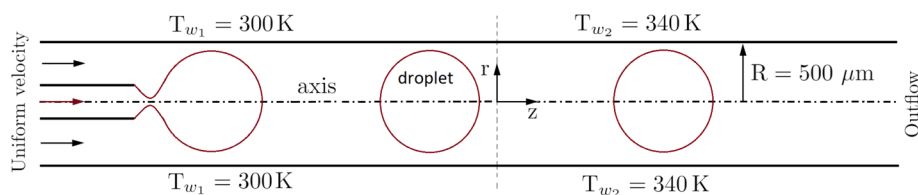
to describe thermal effects and temperature-dependent capillary, where T , c_v , k are, respectively, the temperature field, specific heat capacity at constant volume, and thermal conductivity.

In the phase-field specialization, we assume that the two-phase fluids are immiscible except in a small interfacial region between the phases, which allows mixing and constituents diffusion (see [36]). Furthermore, the liquid phases are treated as incompressible with no phase change and mass transfer across the interface (see., e.g., [22]). The mass density ρ of fluid in each phase is calculated as a smooth function of the phase-field variable φ by

$$\rho = \frac{(1 - \varphi)}{2} \rho_d + \frac{(1 + \varphi)}{2} \rho_c, \quad (3)$$

which allows the unmixed liquids to have different mass densities, ρ_c and ρ_d ; where subscripts d , c refer to dispersed and continuous phases, with $\varphi_d = -1$ and $\varphi_c = 1$. In a similar way, the fluid viscosity ν , specific heat capacity at constant

Fig. 1 Geometric model of the axisymmetric microtube in the co-flowing configuration



volume c_v , and thermal conductivity of fluid in each phase are calculated as follows:

$$v = \frac{(1 - \varphi)}{2} v_d + \frac{(1 + \varphi)}{2} v_c, \quad c_v = \frac{(1 - \varphi)}{2} c_{v_d} + \frac{(1 + \varphi)}{2} c_{v_c},$$

$$k = \frac{(1 - \varphi)}{2} k_d + \frac{(1 + \varphi)}{2} k_c, \tag{4}$$

The Cahn–Hilliard Eq. (1_{3,4}) describes the transport of φ , which is predicted on assuming that the free-energy density is given by a double-well potential with wells at $\varphi_d = -1$ and $\varphi_c = 1$ as:

$$f(\varphi) = \frac{\lambda}{4\varepsilon^2} (\varphi^2 - 1)^2. \tag{5}$$

where λ is the mixing energy per unit of length that can be related to the surface tension σ and interfacial thickness ε as [37]

$$\lambda = \frac{3\sqrt{2}}{4} \varepsilon \sigma. \tag{6}$$

Following Bai et al. [32] and Lim and Lam [38], we assume that the mobility is constant and given by

$$m = \chi \varepsilon^2, \tag{7}$$

where χ is a positive parameter representing a mobility tuning that controls the magnitude of the diffusivity of the phase field. Thus, a large enough value of χ is required to retain a constant interfacial thickness but small enough so that the convective term is not overdamped [38].

In the advective Cahn–Hilliard Eq. (1₃), $m\Delta\mu$ represents a term that minimizes the free energy of the system, which includes higher-order derivatives of φ , designed to keep the interface compact. Note that $m\Delta\mu$ vanishes as m goes to zero, which gives a pure advective transport equation as in the level set method. However, the numerical solution with $m\Delta\mu = 0$ is unstable and of small practical use in most cases. This diffusion term is analogous to numerical diffusion that stabilizes the numerical schemes and improves mass conservation.

The system of Eqs. (1) and (2) introduced above must be supplemented with physically appropriate boundary and initial conditions. The geometry of the co-flowing microtube is assumed to be axisymmetric, as shown in Fig. 1. We therefore adopt the top half of the geometry as a two-dimensional axisymmetric domain. We impose a symmetry boundary condition at the centerline of the microtube domain. We set uniform velocities u_d and u_c and temperature T_{w_1} to the inlet boundary conditions for the continuous and dispersed phases, while the outflow boundary condition with a fixed, zero-pressure constraint $p_0 = 0$, and zero fluxes are imposed to the outlet (see, e.g., [39–41])

$$\mathbf{n} \cdot m \text{ grad} \mu = 0, \quad \mathbf{n} \cdot \text{grad} \varphi = 0, \quad \mathbf{n} \cdot k \text{ grad} T = 0, \tag{8}$$

where \mathbf{n} is the outward-pointing unit vector normal to the boundary. Further, we impose the no-slip, zero velocity $\mathbf{v} = \mathbf{0}$ at the tube wall. Following Fischer et al. [1], we set a temperature distribution as a step function along the microchannel wall, 300 K on the isothermal entrance section and increased to 340 K on the heated section, as shown in Fig. 1. Furthermore, we assume that the liquid thermal behaviors are in thermal equilibrium with the wall at the liquid–solid interface (see, e.g., Gad-el-Hak [42] and Rosengarten et al. [43]). For droplet generation, the phases are set as $\varphi_d = -1$ and $\varphi_c = 1$ at the inlet for dispersed and continuous, respectively. As a consequence, the dispersed phase flow forms a train of droplets; the droplets size and length between droplets can be adjusted by changing the flow rates Q_c when $\varphi_c = 1$ and Q_d when $\varphi_d = -1$. The flow rate ratio α is defined as $\alpha = Q_d/Q_c$ and is used to control the droplets frequency generation.

We identify key controlling parameters of dispersed droplets generator. As in Khater et al. [9], these groups include the physical properties and flow rates of dispersed and continuous phases and the dimensions of microchannel. In our analysis, we will adopt three non-dimensional groups, say the Reynolds number $Re = \rho_c \bar{v}_c R / \nu_c$, capillary number $Ca = \nu_c \bar{v}_c / \sigma$, and flow rate ratio $\alpha = Q_d / Q_c$. These groups are calculated from the dimensional variables that include the volumetric flow rate Q , the viscosity ν , and interfacial tension σ between two immiscible liquids into the microtube, and the radius of the microtube as the characteristic length scale.

3 Numerical method

We have used the finite element software COMSOL Multiphysics to simulate the two-phase droplet and heat transfer in the microtube. In this case, the Navier–Stokes–Cahn–Hilliard and heat transfer Eqs. (1)–(2) are solved using a mixed finite-element method. The Cahn–Hilliard Eq. (1_{3,4}) is handled by adding an auxiliary variable to separate the fourth-order equation into two coupled second-order equations (see, e.g., [39, 41]).

The system of Eqs. (1) and (2) was implemented in the COMSOL Multiphysics using the Laminar Two-Phase Flow Module and coupled with the Heat Transfer Module. For the spatial discretization, we adopt Taylor–Hood elements (see, e.g., Ern and Guermond [44]) that are inf-sup stable elements. Thus, the velocity \mathbf{v} and order parameter φ are interpolated by piecewise-quadratic functions, while the pressure p , chemical potential μ , and temperature T are interpolated by piecewise-linear functions. Furthermore, we apply an implicit second-order BDF method, with free time-stepping controlled by the

solver to take larger or smaller time-steps sizes as required to satisfy the specified tolerances during the computations. At each time-step, the discrete mixed problem results in a system of nonlinear equations that is solved through a fully coupled approach using the damped Newton method. The direct solver PARDISO was selected to solve the discrete system.

3.1 Mesh independence

To study the heat transfer enhancement induced by the two-phase flow within the microchannel, as shown in Fig. 1, immiscible droplet liquid is injected in a co-flowing liquid stream at uniform temperature of 300 K, with the flow rate $Q_c = 64.2 \mu\text{l/s}$, which correspond to the Reynolds number of 50. The flow rate ratio was set at $\alpha = 0.223$, corresponding to a flow rate of $14.3 \mu\text{l/s}$ for the dispersed phase. Those choices have been made to reproduce the results presented in [1] in order to validate our results, as will be discussed in Sect. 4.1. Thus, Table 1 lists the physical properties of the continuous (water) and dispersed (oil PAO) phases used in the numerical simulations. Furthermore, we adopted an interfacial tension value $\sigma_0 = 30 \times 10^{-3} \text{ N/m}$ at 300 K and a temperature coefficient $\kappa = -0.06 \times 10^{-3} \text{ N/(m K)}$, such that the interfacial tension is given by $\sigma = \sigma_0 + \kappa(T - T_{w_1})$; see [1] for details.

As a measure of the heat transfer enhancement caused by the train of two-phase droplets flow, we have used the Nusselt number given by

$$Nu_z = \frac{2Rq|_{w,z}}{k(T_b - T_{w,z})}, \tag{9}$$

where $q|_{w,z}$ is the heat flux at the wall, and the local bulk-mean-temperature T_b is calculated as follows:

$$T_b = \frac{\int_0^R \rho c_v v_z T r dr}{\int_0^R \rho c_v v_z r dr}. \tag{10}$$

The axisymmetric, two-dimensional domain (Fig. 1) is meshed into different structured grids using n_{el} quadrilateral elements. To verify the independence of the results of the mesh choice, we compared the distributions of the normalized axial velocity and dimensionless temperature $\vartheta = (T - T_{w,z}) / (T_b - T_{w,z})$, where $T_{w,z}$ is the wall temperature. As shown in Fig. 2, the axial velocity profiles in five meshes are coincident. The dimensionless temperature

Table 1 Physical properties of the liquids used in the study, see Ref. [45]

Liquid	ρ (kg/m ³)	ν (Pa.s)	c_v (J/kg K)	k (W/m K)
Water	1.0×10^3	1.0×10^{-3}	6.0×10^{-1}	4.2×10^3
Oil (PAO)	8.0×10^2	5×10^{-3}	1.3×10^{-1}	2.3×10^2

distribution presents a deviation between meshes with $n_{el} = 50, 284$ and $70,038$ that are almost negligible, as shown in Fig. 3. Since the two-phase droplet flow increases the local $Nu(z)$ number in comparison to the single-phase flow in the microtube, the Nu number varies periodically in the axial direction. Thus, we adopt the equivalent Nu^* number by space and time averaging Nu to verify the independence of meshes on the convective heat transfer. Figure 4 shows that Nu^* number tends to a plateau value as the number of elements n_{el} grows in the mesh. For the following studies, we employed mesh with $60,757$ elements that satisfy mesh independence, with accuracy and small computational consumption.

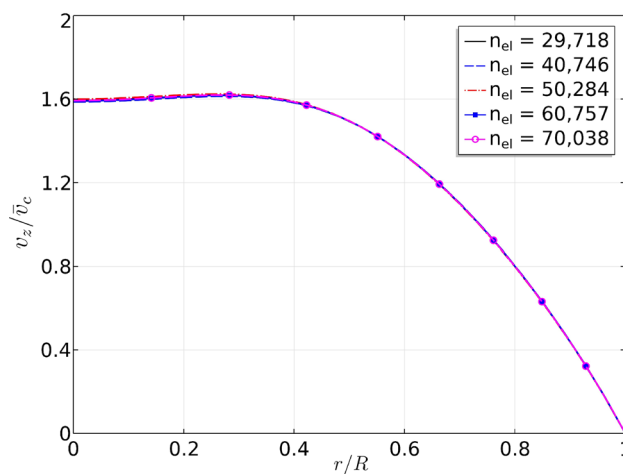


Fig. 2 Normalized axial velocity evaluated at $z = 20R$ for different meshes

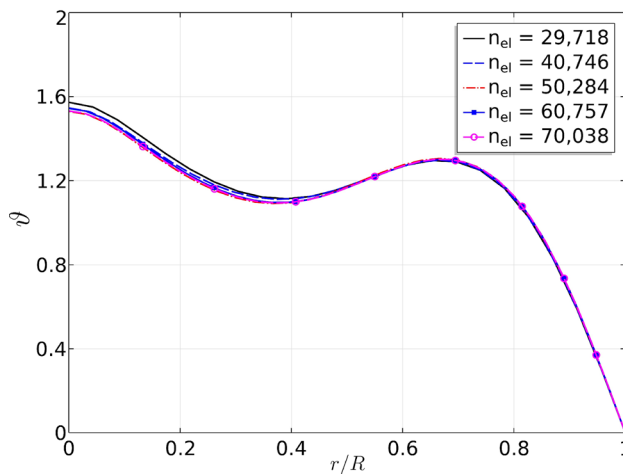


Fig. 3 Dimensionless temperature profiles evaluated at $z = 20R$ for different meshes

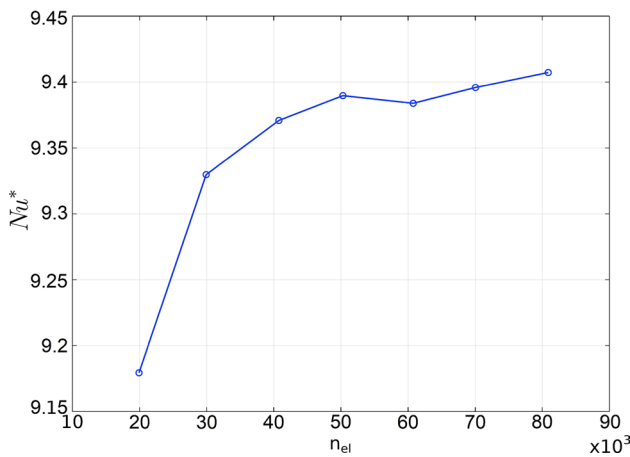


Fig. 4 Average Nusselt number as a function of the number of elements in the mesh

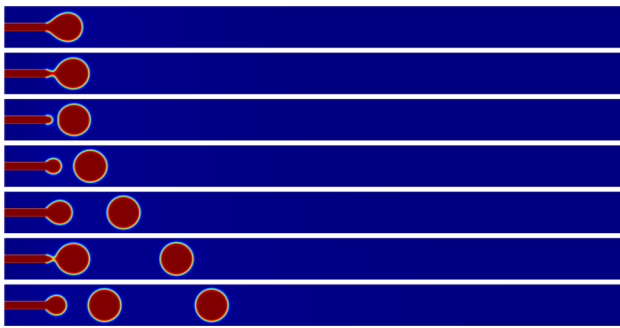


Fig. 5 Snapshots of formation, breakup, and transport of dispersed droplets in the co-flowing microtube for $Q_c = 64.2 \mu\text{l/s}$ and flow rate ratio $\alpha = 0.223$ at different time instant

4 Results and discussion

4.1 Heat transfer enhancement of droplet two-phase flow

The flow patterns results are shown in Fig. 5 at the flow rate of $14.3 \mu\text{l/s}$ for dispersed phase. The dispersed phase generates from the tip of the internal microtube followed up with droplet growth, breakup and transport into the moving continuous phase under a dripping regime. Based on imposed hydrodynamic flow conditions, the simulations predicted that the spherical droplets are distanced by around $3.7R$ from each other and the droplet radius is around $0.8R$, which are in agreement with the flow pattern obtained in the studies by Fischer et al. [1].

The results show convective heat transfer enhancement in the cylindrical microchannel and the influence of droplets frequency and internal circulation zones on the heat transfer rates. We compare the heat transfer rate predicted

from droplets two-phase flow with results presented in the studies by Fischer et al. [1], which the focus was to study the effects of a train droplets on the local Nusselt number, without take into account the droplet generation. Figure 6 shows the local Nusselt number Nu_z and temperature distribution in the axial z -direction at the steady state. As in the studies by Fischer et al. [1], a strongly thermal enhancement is achieved in comparison with a single-phase flow and the Graetz solution. The local Nusselt obtained from the classical approximated solution of the Graetz problem yields $Nu_z = 1.357(PeR/z)^{1/3}$, where $Pe = 2\rho_c \bar{v}_c c_p R/k_c$ is the Peclet number based on the properties of continuous phase.

From Fig. 6, we observe an augmentation of the local Nusselt number profile induced by the velocity of the recirculating zone between droplets being directed from the wall toward the center of the microchannel, meaning a enhancement in the convection transport. These recirculations zones appear periodically in the region between two subsequent droplets, as shown in zones I and III. The temperature distribution in the droplets and continuous phase suggests that the hotter liquid is transported from the heated wall toward the center line of the channel where the liquid is colder. Thus, the liquid in front of the droplets is hotter than the liquid in their tails, with a strong increase in the local Nusselt number. A similar process occurs within the droplets (see region II), where recirculations are observed, as shown in Fig. 7. The predicted local Nu_z along the co-flowing regime in the microtube is in good agreement with the front-tracking-based numerical results obtained by Fischer et al. [1]. The local Nusselt number calculated from the phase-field simulation exhibits a maximum value slightly above 12, in comparison to single-phase flow.

For model validation, we used the root-mean-squared percentage error to measure how well the predicted local Nusselt number agrees with Fischer et al. [1] simulations for liquid–liquid spherical droplets. In short, it is employed the standard formula (see, e.g., Cherbakov et al. [46])

$$\text{Root-mean-squared error} = \sqrt{\frac{\sum_1^n \left(\frac{P-F}{P}\right)^2}{n}} \times 100, \quad (11)$$

where P and F variables represent the predicted and Fischer et al. [1] local Nusselt numbers, respectively, and n is the number of data points. The root-mean-squared percentage error was determined to be around 5.5%.

We consider the effect of dispersed droplets production frequency on the heat transfer enhancement. Figure 8 shows flow patterns predicted at flow rate ratios α ranging from 0.1 to 0.3 (see, e.g., Asthana et al. [47]) in the dripping regime at steady state and fixed capillary number based on the bulk mean velocity $Ca = 2.6 \times 10^{-3}$. Note that increasing the flow

Fig. 6 Variation of Nu and temperature distribution along the co-flowing microtube in single-phase and two-phase droplets flows. The liquid in the droplets is polyalphaolefine (PAO) surrounded by water as continuous phase, with flow rate ratio $\alpha = 0.223$. The simulations are carried out for $Re = 50$ and $Ca = 2.6 \times 10^{-3}$ in the continuous phase. The local Nu of the liquid–liquid droplet flow calculated by Fischer et al. [1]. The root-mean-squared percentage error for the predicted and Fischer et al. simulations was determined to be around 5.5%

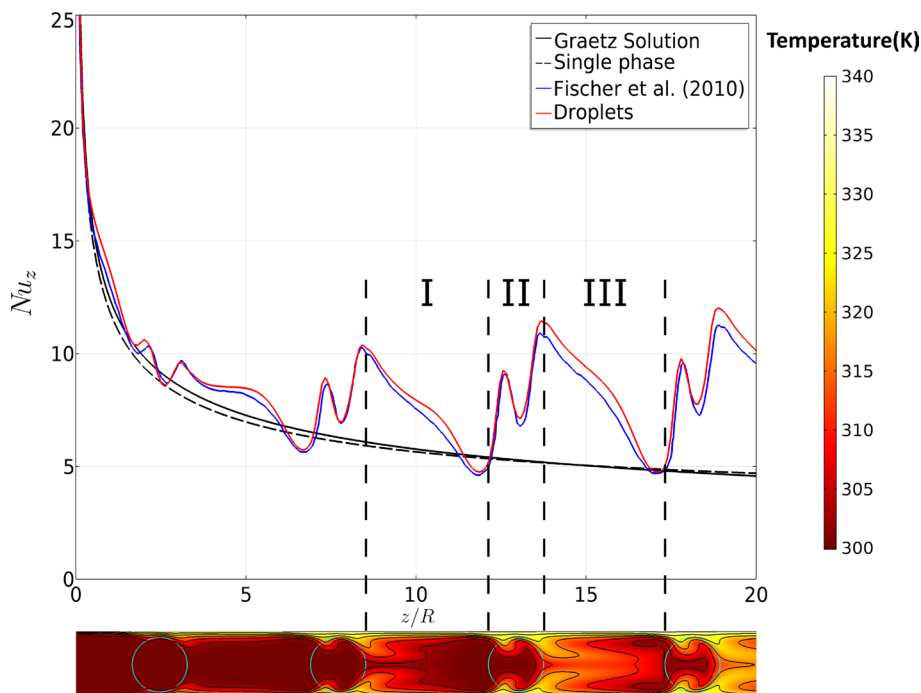


Fig. 7 Streamlines for a moving frame referential with the droplets mean velocity

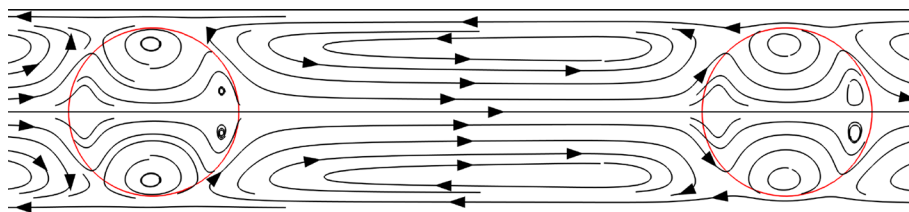
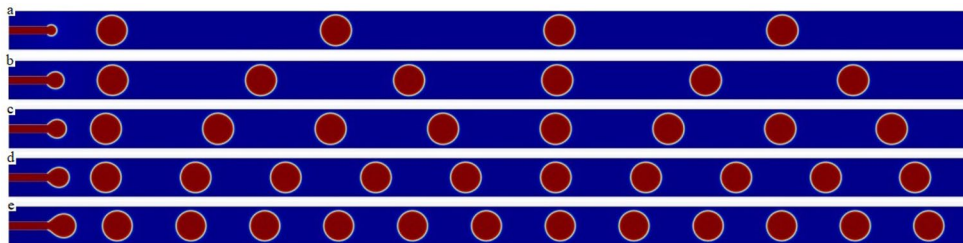


Fig. 8 Flow patterns for different flow rate ratios at the steady state. **a** $\alpha = 0.1$, **b** $\alpha = 0.15$, **c** $\alpha = 0.2$, **d** $\alpha = 0.25$, and **e** $\alpha = 0.3$



rate ratio α , the dispersed-phase frequency increases, and thus, more dispersed droplets flow through the microchannel. Figure 9 shows the influence of the frequency of the dispersed droplets on the temperature field in comparison to the temperature distribution in single-phase flow. The result shows that the convective heat transfer improvement is strongly associated with the distance between droplets in co-flowing. We associate the convective thermal enhancement with the flow structure shortening. The length of flow structures (the distance between droplets) is controlled using five values of the flow rate ratios α to generate different dispersed-phase frequency and flow patterns. From Fig. 9, it can be verified that the temperature distribution between

two droplets is affected in front of the droplet and in the rear of droplets as the flow rate ratio α increases, as shown in Fig. 10, when considering the Nusselt number averaged over time. It is interesting to note that shortening the distance between droplets as increasing the flow rate ratio, the circulating flow between two droplets affects the convective thermal transport.

By introducing the flow-type parameter (Lee et al. [48])

$$\omega = \frac{|D| - |W|}{|D| + |W|}, \tag{12}$$

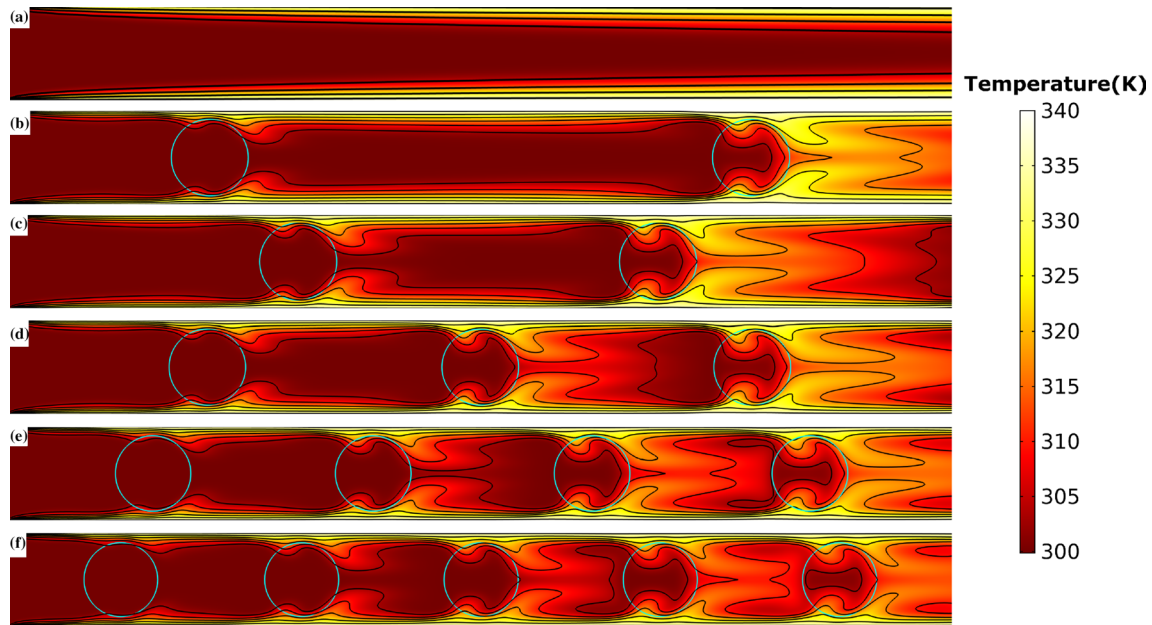


Fig. 9 Temperature distribution for two-phase droplets flows and different flow rate ratios at the steady state. **a** single-phase, **b** $\alpha = 0.1$, **c** $\alpha = 0.15$, **d** $\alpha = 0.2$, **e** $\alpha = 0.25$, and **f** $\alpha = 0.3$. The temperature field of the single-phase flow is added for comparison

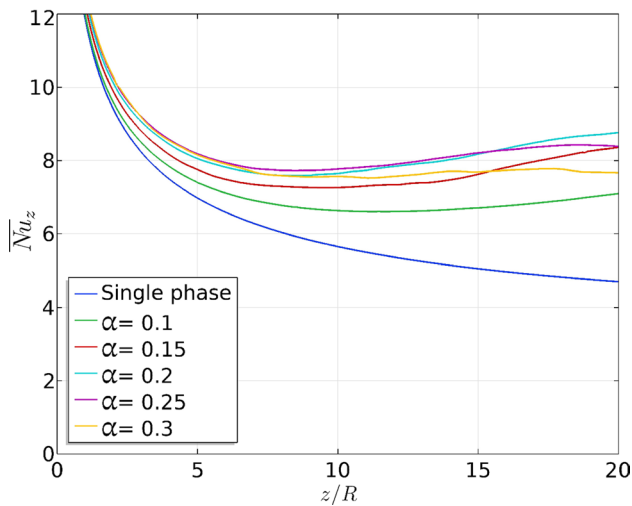


Fig. 10 Nusselt averaged over time for different flow rate ratios α

we quantify the flow structures within and between subsequent droplets, wherein \mathbf{D} represents the symmetric strain rate tensor (stretching) that gives the local deformation and \mathbf{W} is the skew part of the velocity gradient that gives the local rotation in the flow field; their respective magnitudes are defined as $|\mathbf{D}| = \sqrt{\text{tr} \mathbf{D}^2}$ and $|\mathbf{W}| = \sqrt{-\text{tr} \mathbf{W}^2}$ (see, e.g., [49]). The flow-type parameter ω varies from -1 (pure rotational flow) to 1 (pure extensional flow); $\omega = 0$ represents a pure shear flow. The distribution of ω from Fig. 11 evidences the regions where rotation prevails over-stretching rates, regions with $\omega < 0$. When increasing the dispersed-phase

frequency (distance between two droplets shortening), the recirculation structure decreasing in size between subsequent droplets and stretching zones prevails where $\omega > 0$. Thus, from Fig. 9, it can be found that these flow structures (recirculation zones) can affect the convective heat transfer. When compared with the heat transfer in the single-phase flow, we observe an increase of time-averaging Nu number, which suggests a bound limit for the heat transfer enhancement, as shown in Fig. 10. It is interesting to note that after the flow rate ratio reaches a critical value, the Nusselt number starts decreasing. Augmenting the flow rate ratio, the distance between two droplets decreases, presenting a smaller recirculation structure in size between droplets and stretching domains prevails with $\omega > 0$, as shown in Fig. 11.

We find from Fig. 12 the existence of an optimal flow rate ratio, which predicts a maximum heat transfer enhancement of two-phase droplet flow in the microtube.

Figure 13 shows the pressure loss distribution as a function of flow rates. When the average Nu number augments around 34%, we find an increase of about 36.9% of pressure loss at the flow rate of 0.225.

4.2 Effects of capillary on the heat transfer

The Capillary number Ca relates viscous and interfacial forces. For low values of Ca , droplets tend to be elongated because the interfacial tension forces dominate over the actions of the viscous ones. As Ca augments, the breakup droplet rate steadily increases by the effect of the viscous forces accordingly grows, and droplet deformation

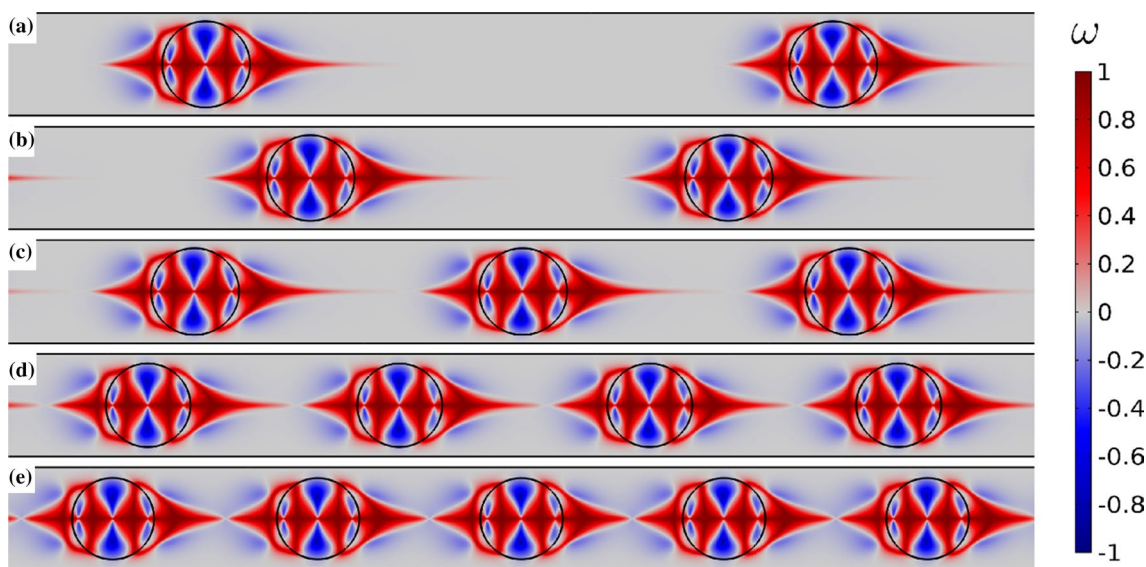


Fig. 11 Flow-type parameter field for **a** $\alpha = 0.1$, **b** $\alpha = 0.15$, **c** $\alpha = 0.2$, **d** $\alpha = 0.25$ and **e** $\alpha = 0.3$

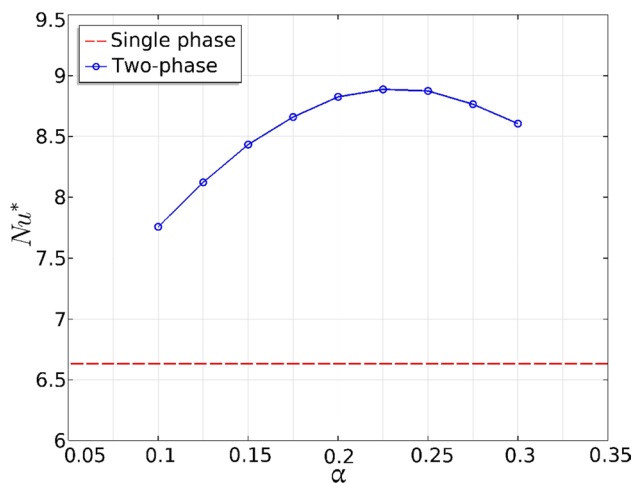


Fig. 12 Nusselt number spatial averaged for different flow rate and single phase (red dashed line)

decreases. For a sufficiently high capillary number, the droplet diameter becomes smaller and spherical droplets are formed, with the shear stress exerted on the droplet more concentrated in one point, as observed in Ref. [50].

Figure 14 shows two-phase droplet flow patterns taking into account different Ca numbers and fixed flow rate ratio. Since the Ca number influences the droplet’s shape and breakup rate, it strongly affects the convective heat transfer, as shown in Fig. 15. As Ca increases, droplets spacing and volume decrease while promoting an initial augmentation in the time-averaging Nusselt number. While Ca continues

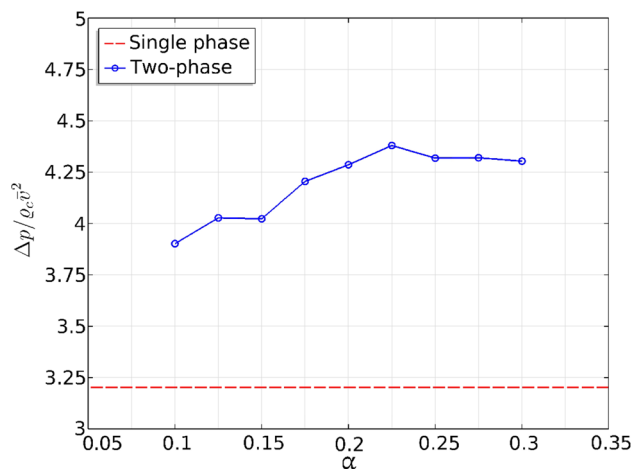


Fig. 13 Dimensionless pressure loss versus flow rate ratio

increasing, droplets become spherical and their diameter progressively smaller, which reduces recirculation between droplets in the dripping regime and, thus, the time-averaging Nusselt number decreases.

Figure 17 shows the dimensionless pressure loss as a function of the flow rate ratio for each value of the Ca number simulated; we find that the pressure loss steadily decreases as Ca augments. It is interesting to note that an optimum scenario regarding the heat transfer enhancement and pressure loss is obtained for $Ca = 2.6 \times 10^{-3}$, as shown in Fig. 16 and 17.

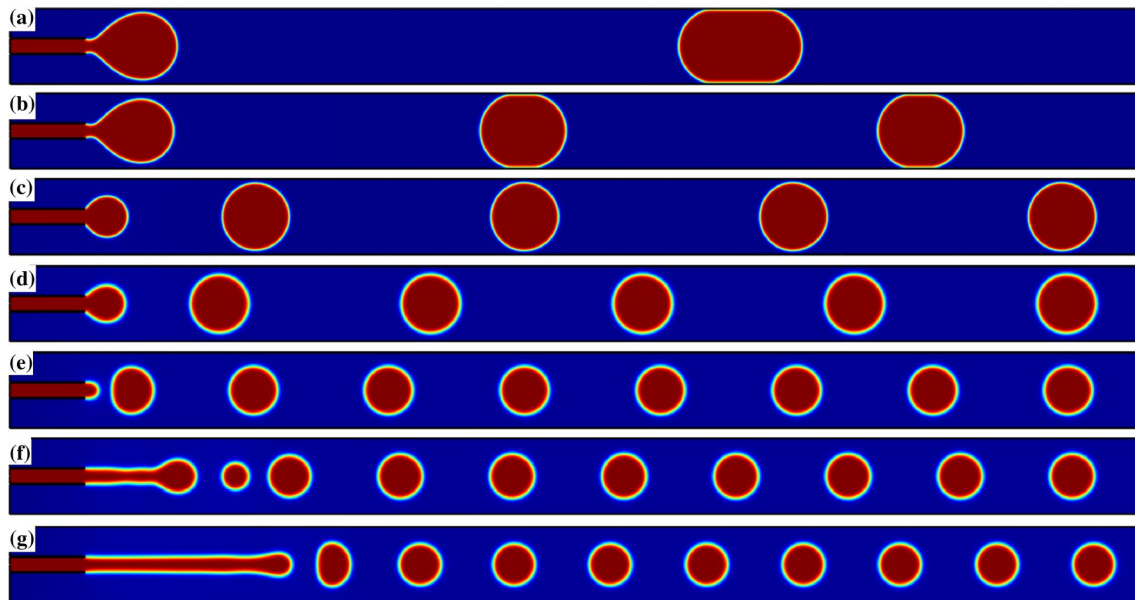


Fig. 14 Droplet formation rate with different Ca and fixed flow rate ratios $\alpha = 0.2$. **a** $Ca = 0.5 \times 10^{-3}$, **b** $Ca = 1 \times 10^{-3}$, **c** $Ca = 2 \times 10^{-3}$, **d** $Ca = 3 \times 10^{-3}$, **e** $Ca = 4 \times 10^{-3}$, **f** $Ca = 5.75 \times 10^{-3}$, and **g** $Ca = 6 \times 10^{-3}$

5 Conclusions

In this work, we employed a phase-field method based on the Navier–Stokes–Cahn–Hilliard equations coupled with the energy equation to simulate the heat transfer enhancement induced by a train of silicone-oil droplets in co-flowing microtube. Different from previous studies, we considered in the simulations droplets formation, breakup, and transport into the thermal entrance region. We found

that with the presence of a train of droplets in the continuous phase flow, the heat transfer can be enhanced with an increase in the pressure loss relative to the single-phase flow. Moreover, the enhancement in the convective heat transfer varies non-monotonically with the flow rate ratio. By augmenting the droplet generation frequency, the distance between droplets decreases, and also the recirculation structure separating droplets, which improves the thermal mixing. Thus, the space-time-averaging Nu number over the heated region increases firstly and then decreases with the flow rate ratio. A comprehensive effect of such observation suggests an optimal flow rate ratio in which the heat transfer enhancement of two-phase droplet flows in the microtube reaches a maximum for the dripping regime. The time-averaging Nu number decreases as the capillary number augments. As a consequence, the heat transfer enhancement decreases since the droplets decrease their size.

As a final remark, numerical simulations compose an outstanding approach to the study of convective heat transfer enhancement induced by two-phase droplet flow in microchannels since they can predict complex two-phase flow conditions free from external interference. However, numerous factors point toward the requirement of a theoretical model for immiscible two-phase flow that accounts for temperature-dependent capillarity to describe the Marangoni effect. Thus, as a work-in-progress, we will propose a non-isothermal phase-field model for immiscible incompressible fluid flows with temperature-dependent capillarity in order to describe the Marangoni effect (or thermo-capillarity convection).

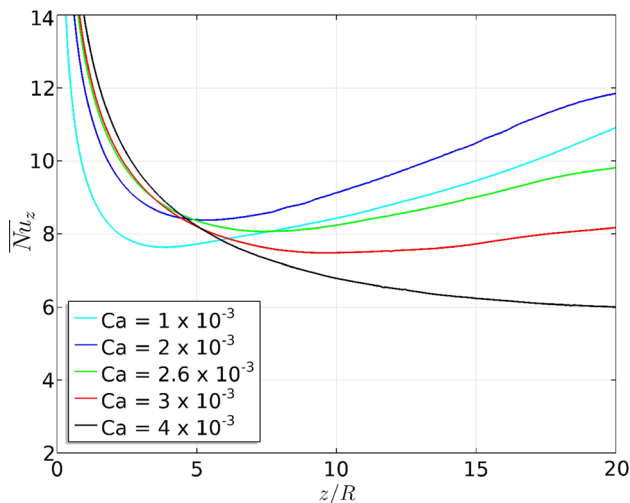


Fig. 15 Nusselt averaged over time for different capillary numbers and flow rate ratios $\alpha = 0.2$

Fig. 16 Effect of flow rate ratio α and capillary number Ca on the spatial average Nusselt number

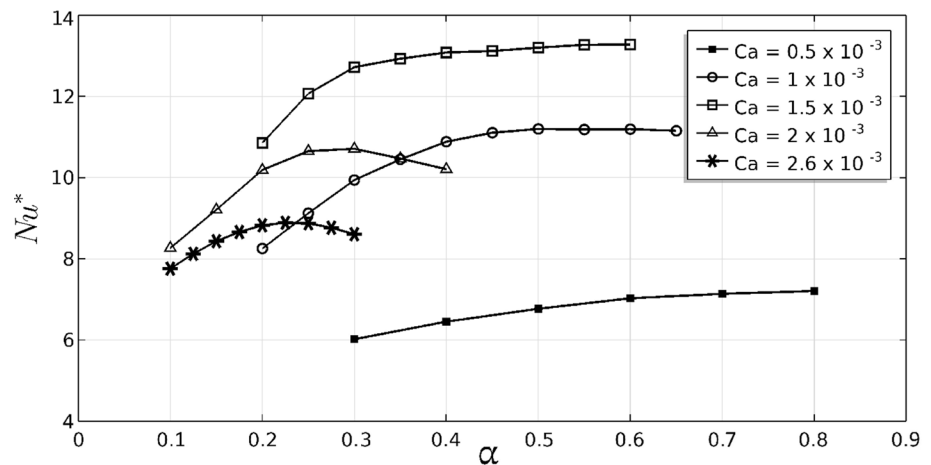
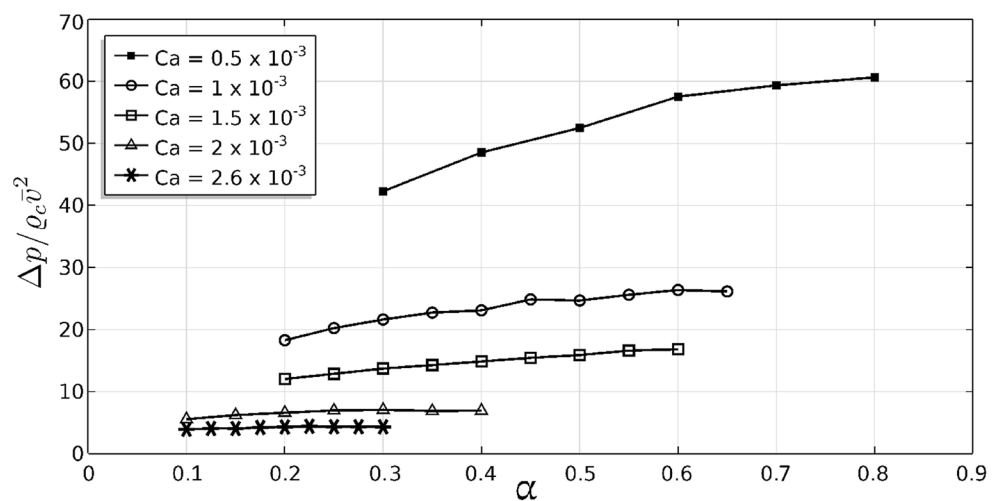


Fig. 17 Dimensionless pressure loss for different flow rate ratios α and capillary number Ca



Acknowledgements The authors acknowledge the Coordenação de Aperfeiçoamento de Pessoal de Nível Superior CAPES for support (Finance Code: 88881.200549/2018-01).

References

- Fischer M, Juric D, Poulikakos D (2010) Large convective heat transfer enhancement in microchannels with a train of coflowing immiscible or colloidal droplets. *J Heat Transf* 132(11):112402
- Bordbar A, Kamali R, Taassob A (2020) Thermal Performance Analysis of Slug Flow in Square Microchannels. *Heat Transf Eng* 41(1):84
- Muzychka Y, Walsh E, Walsh P (2011) Heat transfer enhancement using laminar gas-liquid segmented plug flows. *J Heat Transf* 133(4):041902
- Nguyen NT, Ting TH, Yap YF, Wong TN, Chai JCK, Ong WL, Zhou J, Tan SH, Yobas L (2007) Thermally mediated droplet formation in microchannels. *Appl Phys Lett* 91(8):084102
- Murshed SS, Tan SH, Nguyen NT, Wong TN, Yobas L (2009) Microdroplet formation of water and nanofluids in heat-induced microfluidic T-junction. *Microfluid Nanofluid* 6(2):253
- Zhu P, Wang L (2017) Passive and active droplet generation with microfluidics: a review. *Lab Chip* 17(1):34
- Stan CA, Tang SK, Whitesides GM (2009) Independent control of drop size and velocity in microfluidic flow-focusing generators using variable temperature and flow rate. *Anal Chem* 81(6):2399
- Yesiloz G, Boybay MS, Ren CL (2017) Effective thermo-capillary mixing in droplet microfluidics integrated with a microwave heater. *Anal Chem* 89(3):1978
- Khater A, Mohammadi M, Mohamad A, Nezhad AS (2019) Dynamics of temperature-actuated droplets within microfluidics. *Sci Rep* 9(1):1
- Lovrić A, Dettmer WG, Perić D (2019) Low order finite element methods for the Navier–Stokes–Cahn–Hilliard equations. [arXiv:1911.06718](https://arxiv.org/abs/1911.06718)
- Santra S, Mandal S, Chakraborty S (2020) Phase-field modeling of multicomponent and multiphase flows in microfluidic systems: a review. *Int J Numer Methods Heat Fluid Flow* 31(10):3089
- Glimm J, Klingenberg C, McBryan O, Plohr B, Sharp D, Yaniv S (1985) Front tracking and two-dimensional Riemann problems. *Adv Appl Math* 6(3):259
- Tryggvason G, Bunner B, Esmaeili A, Juric D, Al-Rawahi N, Tauber W, Han J, Nas S, Jan YJ (2001) A front-tracking method for the computations of multiphase flow. *J Comput Phys* 169(2):708

14. Prosperetti A, Tryggvason G (2009) Computational methods for multiphase flow. Computational methods for multiphase flow. Cambridge University Press, Cambridge
15. Gross S, Reusken A (2011) Numerical methods for two-phase incompressible flows, vol 40. Springer, Berlin
16. Hirt CW, Nichols BD (1981) Volume of fluid (VOF) method for the dynamics of free boundaries. *J Comput Phys* 39(1):201
17. Wang Z, Yang J, Stern F (2012) A new volume-of-fluid method with a constructed distance function on general structured grids. *J Comput Phys* 231(9):3703
18. Bellotti T, Theillard M (2019) A coupled level-set and reference map method for interface representation with applications to two-phase flows simulation. *J Comput Phys* 392:266
19. Gibou F, Fedkiw R, Osher S (2018) A review of level-set methods and some recent applications. *J Comput Phys* 353:82
20. Theillard M, Gibou F, Saintillan D (2019) Sharp numerical simulation of incompressible two-phase flows. *J Comput Phys* 391:91
21. Gurtin ME, Polignone D, Vinals J (1996) Two-phase binary fluids and immiscible fluids described by an order parameter. *Math Models Methods Appl Sci* 6(06):815
22. Abels H, Garcke H, Grün G (2012) Thermodynamically consistent, frame indifferent diffuse interface models for incompressible two-phase flows with different densities. *Math Models Methods Appl Sci* 22(03):1150013
23. Cahn JW, Hilliard JE (1959) Free energy of a nonuniform system. III. Nucleation in a two-component incompressible fluid. *J Chem Phys* 31(3):688
24. Cahn JW (1962) On spinodal decomposition in cubic crystals. *Acta Metall* 10(3):179
25. Allen SM, Cahn JW (1972) Ground state structures in ordered binary alloys with second neighbor interactions. *Acta Metall* 20(3):423
26. De Menech M (2006) Modeling of droplet breakup in a microfluidic T-shaped junction with a phase-field model. *Phys Rev E* 73(3):031505
27. Zhou C, Yue P, Feng JJ (2006) Formation of simple and compound drops in microfluidic devices. *Phys Fluids* 18(9):092105
28. Ganapathy H, Al-Hajri E, Ohadi MM (2013) Phase field modeling of Taylor flow in mini/microchannels, part I: bubble formation mechanisms and phase field parameters. *Chem Eng Sci* 94:138
29. Ganapathy H, Al-Hajri E, Ohadi MM (2013) Phase field modeling of Taylor flow in mini/microchannels, part II: hydrodynamics of Taylor flow. *Chem Eng Sci* 94:156
30. Kamrani S, Mohammadi A (2020) Controlling the microscale separation of immiscible liquids using geometry: a computational fluid dynamics study. *Chem Eng Sci* 220:115625
31. Li R, Gao Y, Chen J, Zhang L, He X, Chen Z (2020) Discontinuous finite volume element method for a coupled Navier–Stokes–Cahn–Hilliard phase field model. *Adv Comput Math* 46(2):1
32. Bai F, He X, Yang X, Zhou R, Wang C (2017) Three dimensional phase-field investigation of droplet formation in microfluidic flow focusing devices with experimental validation. *Int J Multiph Flow* 93:130
33. Moezzi M, Kazemzadeh Hannani S, Farhanieh B (2019) The role of surface wettability on the heat transfer in liquid-liquid two-phase flow in a microtube. *Phys Fluids* 31(8):082004
34. Christopher GF, Anna SL (2007) Microfluidic methods for generating continuous droplet streams. *J Phys D Appl Phys* 40(19):R319
35. Deen WM (1998) Analysis of transport phenomena, vol 2. Oxford University Press, New York
36. Liang Z, Niu Q, Shuai J (2020) Energy equality for weak solutions to Cahn–Hilliard/Navier–Stokes equations. *Appl Math Lett* 99:105978
37. Yue P, Feng JJ, Liu C, Shen J (2004) A diffuse-interface method for simulating two-phase flows of complex fluids. *J Fluid Mech* 515:293
38. Lim CY, Lam YC (2014) Phase-field simulation of impingement and spreading of micro-sized droplet on heterogeneous surface. *Microfluid* 17(1):131
39. Gomez H, Hughes TJ (2011) Provably unconditionally stable, second-order time-accurate, mixed variational methods for phase-field models. *J Comput Phys* 230(13):5310
40. Dong S (2012) On imposing dynamic contact-angle boundary conditions for wall-bounded liquid-gas flows. *Comput Methods Appl Mech Eng* 247:179
41. Yang Z, Lin L, Dong S (2019) A family of second-order energy-stable schemes for Cahn–Hilliard type equations. *J Comput Phys* 383:24
42. Gad-el Hak M (2005) Differences between liquid and gas transport at the microscale. *Techn Sci* 53(4):301–316
43. Rosengarten G, Cooper-White J, Metcalfe G (2006) Experimental and analytical study of the effect of contact angle on liquid convective heat transfer in microchannels. *Int J Heat Mass Transf* 49(21–22):4161
44. Ern A, Guermond JL (2013) Theory and practice of finite elements, vol 159. Springer, Berlin
45. Mohapatra SC, Loikits D (2005) In: Semiconductor thermal measurement and management IEEE twenty first annual IEEE symposium, 2005. IEEE, pp 354–360
46. Shcherbakov MV, Brebels A, Shcherbakova NL, Tyukov AP, Janovsky TA, Kamaev VA (2013) A survey of forecast error measures. *World Appl Sci J* 24(24):171
47. Asthana A, Zinovik I, Weinmueller C, Poulidakos D (2011) Significant Nusselt number increase in microchannels with a segmented flow of two immiscible liquids: an experimental study. *Int J Heat Mass Transf* 54(7–8):1456
48. Lee JS, Dylla-Spears R, Teclemariam NP, Muller SJ (2007) Microfluidic four-roll mill for all flow types. *Appl Phys Lett* 90(7):074103
49. Gurtin ME, Fried E, Anand L (2010) The mechanics and thermodynamics of continua. Cambridge University Press, Cambridge
50. Li X, He L, Qian P, Huang Z, Luo C, Liu M (2021) Heat transfer enhancement of droplet two-phase flow in cylindrical microchannel. *Appl Therm Eng* 186:116474

Publisher's Note Springer Nature remains neutral with regard to jurisdictional claims in published maps and institutional affiliations.